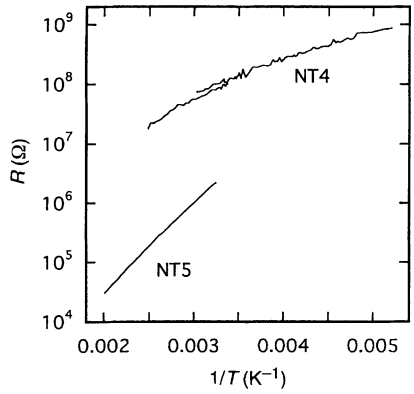

FIG. 3 Semilogarithmic plot of the resistance of nanotubes 4 and 5 (see Table 1) versus the inverse of the temperature (traces labelled NT4 and NT5 are four-probe and two-probe results, respectively).

suggests a more complex behaviour. Further analyses of more tubes are needed to clarify this temperature dependence.

Some nanotubes show large transitions with temperature and they may occur in either direction. The sudden increase in resistance with decreasing temperature in NT6 and NT1 might be due to a Peierls transition, while the profile of NT7a could be due to an insulator-to-metal transition. Further investigation of such transitions will be necessary to establish their exact identity. These transitions may be the property of either one or more shells in the tube and/or a segment of the tube as the comparison of Fig. 2*b* and *f* clearly illustrates. Therefore the observed conductivity of a single nanotube, even by a four-probe measurement, may sometimes be the sum of various segments in series between the probes.

Langer *et al.*[11] have studied the conductance of a non-annealed 20-nm nanotube in a two-probe configuration. In contrast to the slight positive magneto-resistance and small linear temperature dependence in our samples, they reported a strong negative magneto-resistance and a logarithmic fall in resistance ($R(T) \approx -\log(T)$) with increasing temperature. Their results were attributed to weak localization in a disordered two-dimensional conductor[11]. The difference could be simply be part of the wide spectrum of nanotube types. It is already well established that the bulk properties of nanotubes vary significantly depending on where they were made, which of course reflects a variation of the distribution of the types of individual tubes composing the bulk[9,10]. The difference could also stem from the methodology used in preparing the tube for transport measurements. Since submission of this paper, another two-probe study of nanotubes has been published[15]. Comparison of the measured resistances with our results is difficult because no temperature or magnetic field dependence were reported and the nanotubes were produced catalytically.

The presence of both metallic and non-metallic nanotubes in these samples is consistent with theoretical predictions that single nanotubes may be metallic or semiconducting depending on their helicity[2–5], and that this should be observable for nanotubes with diameters up to 30 nm for the wide-gap semiconducting types[5]. In multi-layer nanotubes such as these studied here, the metallic and semiconducting nature of the tubes are expected to be modified by the interlayer interactions[7,16]. Furthermore, we cannot unequivocally rule out the possibility that structural defects do not contribute to the observed behavior, even though we used annealed arc-produced nanotubes. Such factors probably contribute to the large variations observed in the resistivity between the metallic tubes. Combined with the appearance of abrupt changes in resistivity with temperature, it clearly shows that nanotubes have a far wider spectrum of electronic properties than had been expected. Each nanotube is unique, demonstrating the strong correlation of structure and electronic properties at this scale. □

Received 2 April; accepted 11 June 1996.

1. Mintmire, J. W., Dunlap, B. I. & White, C. T. *Phys. Rev. Lett.* **68,** 631–634 (1992).
2. Hamada, N., Sawada, A. & Oshiyama, A. *Phys. Rev. Lett.* **68,** 1579–1581 (1992).
3. Saito, R., Fujita, M., Dresselhaus, G. & Dresselhaus, M. S. *Appl. Phys. Lett.* **60,** 2204–2206 (1992).
4. Tanaka, K., Okahara, K., Okada, M. & Yamabe, T. *Chem. Phys. Lett.* **191,** 469–472 (1992).
5. White, C. T., Robertson, D. H. & Mintmire, J. W. *Phys. Rev.* B**47,** 5485–5488 (1993).
6. Jishi, R. A., Dresselhaus, M. S. & Dresselhaus, G. *Phys. Rev.* B**48,** 11385–11389 (1993).
7. Lambin, Ph., Philippe, L., Charlier, J. C. & Michenaud, J. P. *Computat. Mater. Sci.* **2,** 350–356 (1994).
8. Blase, X., Benedict, L. X., Shirley, E. L. & Louie, S. G. *Phys. Rev. Lett.* **72,** 1878–1881 (1994).
9. Ebbesen, T. W. *A. Rev. Mater. Sci.* **24,** 235–264 (1994).
10. Kosaka, M., Ebbesen, T. W., Hiura, H. & Tanigaki, K. *Chem. Phys. Lett.* **233,** 47–51 (1995).
11. Langer, L. *et al. Phys. Rev. Lett.* **76,** 479–482 (1996).
12. Ebbesen, T. W. & Ajayan, P. M. *Nature* **358,** 220–222 (1992).
13. Primak, W. & Fuchs, L. H. *Phys. Rev.* **95,** 22–30 (1954).
14. Dresselhaus, M. S., Dresselhaus, G., Sugihara, K., Spain, I. L. & Goldberg, H. A. in *Graphite Fibers and Filaments* (eds Gonser, U., Mooradian, A., Muller, K. A., Panish, M. B. & Sakaki, H.) 173–229 (Springer, New York, 1988).
15. Dai, H., Wong, E. W. & Lieber, C. M. *Science* **272,** 523–526 (1996).
16. Benedict, L. X., Crespi, V. H., Louie, S. G. & Cohen, M. L. *Phys. Rev.* B**52,** 14935–14939 (1995).

ACKNOWLEDGEMENTS. We thank D. J. Chadi and N. S. Wingreen for their comments on these results, and A. Dziesiaty, W. Muth, H. Gieser and H. Zimmermann for their assistance.

CORRESPONDENCE should be addressed to T.W.E. and H.J.L.

El Niño-like climate change in a model with increased atmospheric CO_2 concentrations

Gerald A. Meehl & Warren M. Washington

National Center for Atmospheric Research, Boulder, Colorado 80307-3000, USA

Sea surface temperatures in the tropical Pacific Ocean increased on average by serveral tenths of a degree during the 1980s and early 1990s[1–4], contributing to the observed global warming during this period[5]. Here we investigate the possible causes of this Pacific warming, using a global coupled ocean–atmosphere general circulation model incorporating increasing concentrations of atmospheric carbon dioxide. In the model, cloud cover and cloud albedo feedbacks contribute to tropical Pacific sea surface temperature increases that are greater east of 180° longitude, with attendant shifts in large-scale precipitation patterns and mid-latitude circulation anomalies in the north Pacific. These anomalies resemble some aspects of El Niño events, as well as features associated with recent observed Pacific-region climate anomalies. The resemblance to El Niño complicates the problem of detection and attribution of climate change, and suggests that depletion of freshwater resources[6] may be an additional hazard of greenhouse warming for populations in the western Pacific region.

A second-generation global coupled general circulation climate model was integrated for 75 years with atmospheric CO_2 levels increasing at a rate of 1% per year compounded. The last 20 years of this experiment are analysed (years 56–75; the CO_2 level doubles at approximately year 70) and compared to a control integration averaged over that same period with present-day amounts of CO_2. No flux corrections are used at the air–sea interface in the coupled model. The observed area-averaged sea surface temperature (SST) difference, western minus eastern Pacific area (as defined in Table 1), is 4.19 °C, and the coupled model difference is 3.21 °C. Thus the model is able to maintain a

reasonable longitudinal SST gradient across the Pacific albeit with mean SSTs somewhat warmer than observed (Table 1; also Fig. 3*a* in ref. 7).

A simple cloud albedo feedback parametrization and a mass flux convective scheme are included in the atmospheric model. The latter represents the super greenhouse effect in the model[7,8]. The former parametrization accounts for the observed relationship between very warm SSTs, deep convection and bright clouds[8,9] such that if SST is >303 K *and* deep convection is taking place at that gridpoint, middle- and upper-level convective cloud albedos (starting at 0.3 and 0.15, respectively) increase linearly to 0.6 for the SST range of 303–308 K. Though the total greenhouse effect increases rapidly for SST values above ~300 K (ref. 8) thus suggesting an active cloud albedo feedback for SST above 300 K, we use the more conservative SST threshold of 303 K for our cloud albedo feedback parametrization. This SST

TABLE 1 Area averages from the coupled model

	SST (°C)	Abs. Solar ($W m^{-2}$)	Net IR ($W m^{-2}$)	Sens. ($W m^{-2}$)	Latent ($W m^{-2}$)	Adv. ($W m^{-2}$)	Q-con. (%)	Q (%)	TCLD (%)	Alb. (%)
E. Pacific	+3.49	+2.23	+0.92	+2.11	+8.67	+7.65	+62	+22	−13	−4
W. Pacific	+2.21	−3.92	+0.28	+0.88	+0.81	+5.28	+3	+16	−5	+1

The western tropical Pacific area is defined for 5° S–5° N, 140° E–170° E, and the eastern tropical Pacific area is defined for 5° S–5° N, 120° W–90° W. Computed minus observed[33] area averaged SST differences for the control case are 1.89 °C for the eastern Pacific area, and 0.91 °C for the western Pacific area, with the coupled model somewhat systematically warmer than observed as noted in the text and elsewhere[7]. To compare the effects of the cloud albedo feedback on the longitudinal SST response across the tropical Pacific to an increase of CO_2, we note that the eastern Pacific area-averaged SSTs in the first column warm 58% more than the western Pacific area-averaged SSTs. In contrast, the eastern Pacific area warms only 30% more that the western Pacific area in a different version of the coupled model without cloud albedo feedback[34]. In a version of the atmospheric model coupled to a non-dynamic slab ocean[9] the east Pacific area warmed 20% more than the western Pacific area when cloud albedo feedback was included, but only 5% more without cloud albedo feedback. Using a sample from April (following Fig. 1) from the present coupled model both with and without the cloud albedo scheme, the change in total absorbed solar radiation at the top of the atmosphere for the western Pacific area with cloud albedo feedback is $-5.1\,W m^{-2}$. The contribution due to changes in cloud albedo alone from the cloud albedo feedback scheme (the difference in C_s at the top of the atmosphere with and without the cloud albedo feedback scheme) is $-11.9\,W m^{-2}$. Thus the contribution due to cloud decreases is $+6.8\,W m^{-2}$. In the eastern Pacific area, decreases in cloud fraction (increased convective cloud with smaller grid fraction coverage) contribute to increased absorbed solar radiation ($+13.8\,W m^{-2}$), but there is also a contribution from increased cloud albedo of $-7.2\,W m^{-2}$ (the difference in C_s with and without the cloud albedo feedback scheme). Thus the contribution due to cloud changes is $+21.0\,W m^{-2}$. There is 65% more solar radiation reflected by the clouds in the west compared to the east solely due to the cloud albedo feedback in the model, but there are also contributions from changes in cloud amount and type in response to the dynamical coupling between ocean and atmosphere. Without cloud albedo feedback and ocean dynamics, the major contributor to decreasing east–west SST gradient is temperature–evaporation feedback that can produce similar El Niño-like climate-change signals associated with tropical Pacific warming[34,35]. Shown in this table are area-averaged results for increased CO_2 experiment minus control for the present version of the coupled model, December–January–February, 20-year averages. Total cloud and albedo for the eastern Pacific area control case are 0.61 and 0.23, respectively, while those quantities for the western Pacific area control case are 0.79 and 0.28, respectively. Abbreviations used: absorbed solar at the surface (abs.solar), net infrared at the surface (net IR), sensible (sens.), latent and ocean heat advection (adv.); surface moisture convergence (Q-con.), surface moisture (Q), total cloud amount (TCLD), and albedo (alb.).

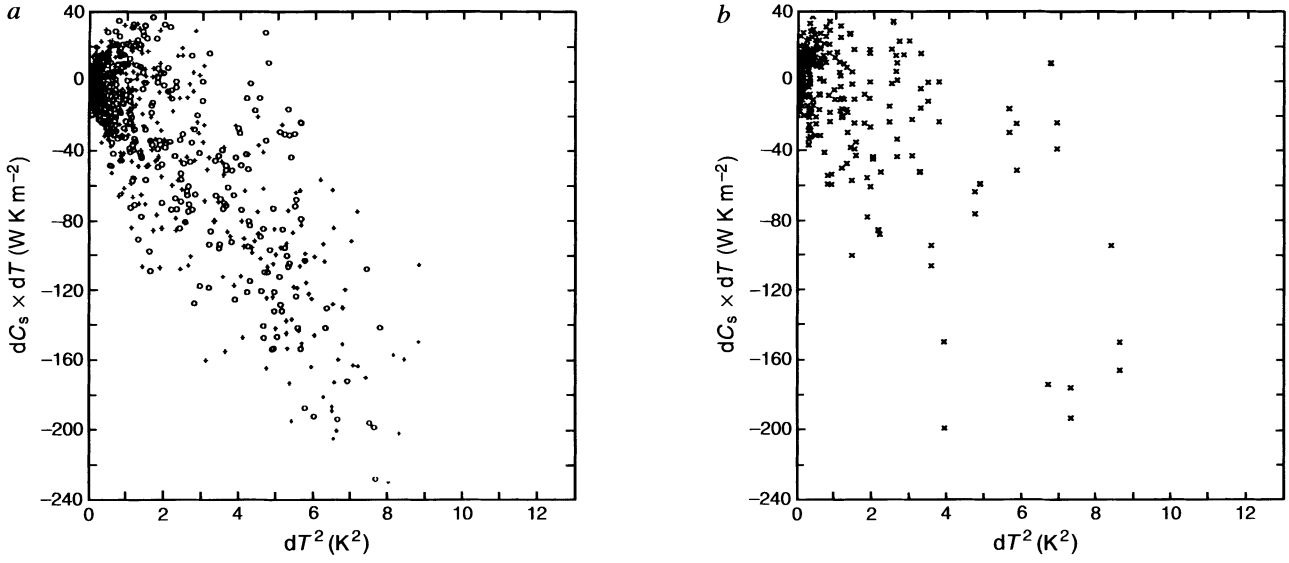

FIG. 1 *a*, Relative change in solar absorption by the ocean–atmosphere system between warm and cold periods, as measured. Plotted points are the product of the change in SST (dT) and change in cloud radiative forcing at the top of the atmosphere (dC_s as in ref. 8) versus the square of the change in SST (dT^2) for each 2.5° × 2.5° region for a warm (April 1987) minus cold (April 1984) period (+ symbols), and a cold (April 1989) minus warm (April 1987) period (O symbols) in the observations over the tropical pacific from 10° N to 10° S (ref. 8). Values are plotted for dC_s × dT less than $+40\,W m^{-2}$ and greater than $-240\,W m^{-2}$, and dT^2 values between 0 and $13\,K^2$. The linear least-squares fit is $dC_s/dT = -19\,W m^{-2}\,K^{-1}$ ($r = -0.80$). *b*, As *a* but from the the model formulated in exactly the same way except for each 4.5° × 7.5° region (thus there are less samples than in *a*) for a warm (April, year 63) minus cold (April year 66) period in the equatorial eastern Pacific, and a cold (April year 58) minus warm (April year 63) period in the control run. The linear fit is $dC_s/dT = -13\,W m^{-2}\,K^{-1}$ with $r = -0.60$. Both observations and the model show a similar relationship with a negative value for the product indicating a decrease (increase) in absorbed solar energy with a warming (cooling) of the ocean.

threshold can be related physically to static energy considerations such that a surface parcel with SST of 303 K has increased boundary-layer moisture and can be estimated to penetrate through the depth of the tropical troposphere (thus increasing water/ice content and producing brighter middle and high clouds). A surface parcel with, for example, SST of 297 K has less boundary-layer moisture and is only likely to penetrate to the middle troposphere with proportionately less increases of water/ice content in clouds at that level[8].

Even though the cloud effects in the present model are simply accounted for, their inclusion compares favourably to a model with a computed cloud optical properties feedback scheme[10] and also reasonably reproduces observed measures of cloud albedo feedback and the super greenhouse effect[7,8]. A further validation of the simple cloud albedo feedback scheme (Fig. 1) shows that the observed change in cloud shortwave forcing (dC_s) as a function of change in SST (dT) for warm compared to cold episodes in the tropical Pacific (Fig. 1*a*) produces a linear fit of $-19\,W\,m^{-2}\,K^{-1}$ ($r = -0.80$). A directly comparable plot for the model (with fewer samples owing to a coarser sampling grid, Fig. 1*b*) reveals a value of $dC_s/dT = -13\,W\,m^{-2}\,K^{-1}$ ($r = -0.60$).

Owing to the uncertainties involved with some cloud processes, cloud feedbacks can be adjusted to produce a wide variety of sensitivities[11]. But because we do not know all the details of the climate-system response to future changes of forcing, we must assume that parametrizations adjusted to represent present-day conditions (such as the one involving an SST threshold for cloud albedo feedback) would apply to a future climate state. This assumption may not be warranted, and is an important caveat to be kept in mind in this experiment and in any model simulation of climate change with simple parametrizations that represent sometimes controversial interpretations of present-day conditions[12,13].

SST anomalies in the tropical Pacific region, increased CO_2 minus control, for the December–January–February season (this season is shown here owing to observational studies that have focused on this season; other seasons in the model show

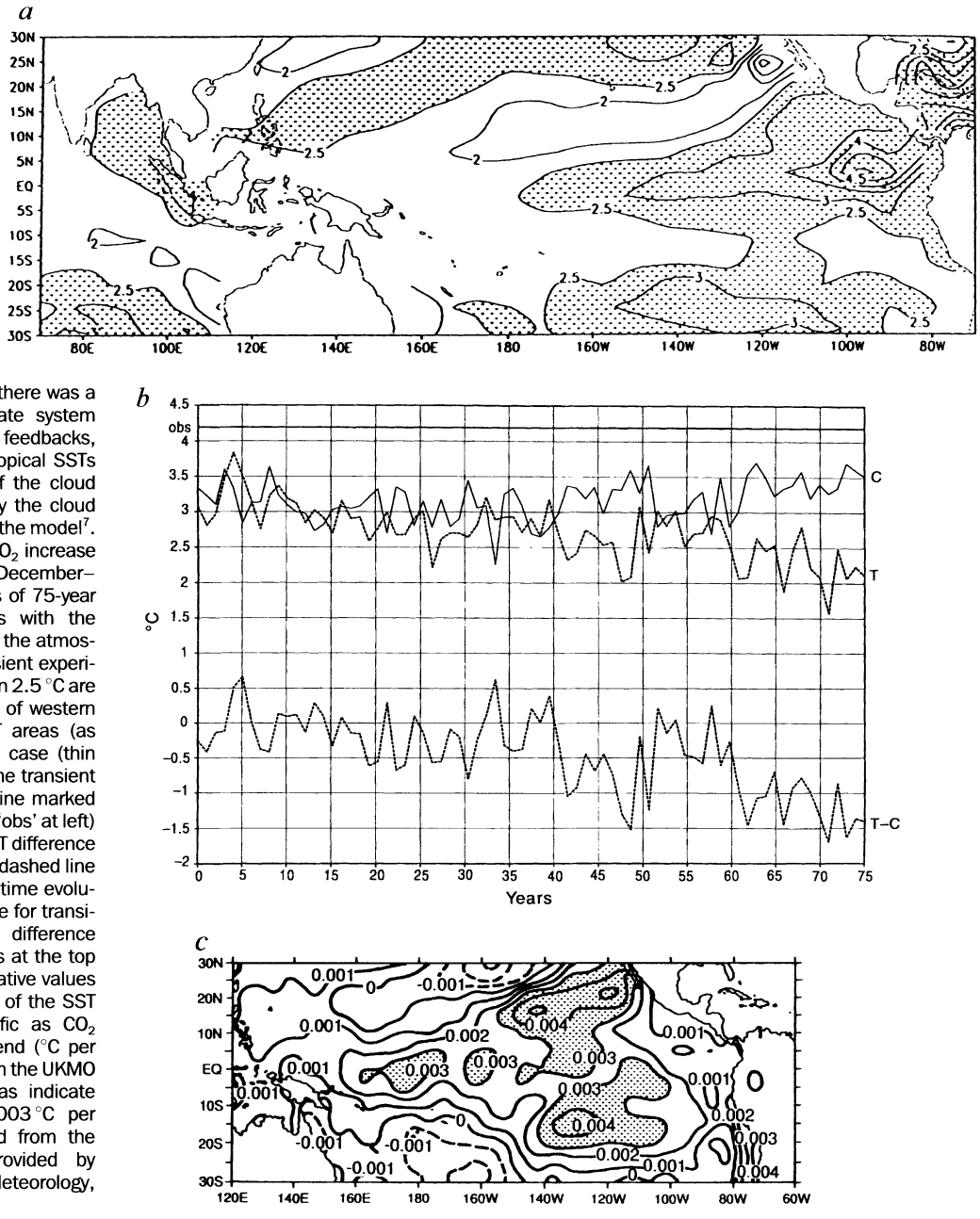

FIG. 2 Changes in tropical Pacific SSTs from the coupled model and observations. In the coupled model, the atmospheric model has an approximate horizontal resolution of 4.5° latitude and 7.5° longitude with nine vertical levels, the ocean and sea-ice components have 1° latitude–longitude resolution with 20 levels in the ocean, sea ice includes a three-layer thermodynamic scheme along with dynamic sea ice. A sensitivity experiment performed with this version of the coupled model where the cloud albedo feedback was strengthened showed that (1) there was a large-scale response of the climate system combining radiative and dynamic feedbacks, and (2) the maximum values of tropical SSTs were a function of the strength of the cloud albedo feedback as represented by the cloud albedo feedback parametrization in the model[7]. *a*, SST differences (°C), transient CO_2 increase experiment minus control, for December–January–February, the last 20 years of 75-year transient and control integrations with the coupled model (CO_2 has doubled in the atmosphere at about year 70 of the transient experiment), areas of warming greater than 2.5 °C are stippled; *b*, at top, the time series of western Pacific minus eastern Pacific SST areas (as defined in Table 1) for the control case (thin solid line marked 'C' at right) and the transient CO_2 increase experiment (dashed line marked 'T' at right), thick solid line (marked 'obs' at left) is the observed west-minus-east SST difference as noted in the text; at bottom, the dashed line (marked 'T-C' at right) denotes the time evolution of the west–east SST difference for transient minus control cases (the difference between the solid and dashed lines at the top of the panel), with increasingly negative values indicating a progressive slackening of the SST gradient across the tropical Pacific as CO_2 increases in the model; *c*, SST trend (°C per month) for the period 1970–91 from the UKMO GISST dataset[18,29,30], stippled areas indicate warming trends greater than 0.003 °C per month (SST trend map generated from the GISST dataset cited above, provided by M. Latif, Max Planck Institute for Meteorology, Hamburg, Germany).

similar results) show less warming (<2 °C, Fig. 2*a*) where mean SSTs are greatest in the model[7]. Meanwhile in the tropical Pacific east of the Date Line, there is relatively greater warming of the ocean surface (2–4 °C). Therefore, the CO_2-related surface warming is not uniform at the ocean surface across the tropical Pacific. There is a reduction of the east–west or zonal SST gradient along the Equator and immediately to the north, with somewhat less reduction to the south. This slackened equatorial zonal SST gradient is not unlike what is seen during El Niño events[14–17]. This is not due to a first-order change of frequency of El Niño events in the model, as preliminary results from an analysis of El Niño frequency do not show significant changes between control and increased-CO_2 experiments. A time series of area-averaged differences between eastern and western tropical Pacific SSTs shows a steady decrease of east–west SST gradient throughout the course of the 75-year experiments with increased CO_2 (Fig. 2*b*).

Observational studies have shown that the SST warming that occurred during the 1980s was not uniform over the tropical Pacific region[3,17,18]. During this time period when global temperatures also increased, the area-averaged mean warming for the tropical western Pacific (~0.15 °C over an area from 120° E to 170° W, 20° N to 20° S) was roughly less than half that in the tropical eastern Pacific (~0.35 °C for the area 170° W–coasts of Central and South America, 20° N to 20° S)[18]. SST trends from 1970 to 1991 (Fig. 2*c*) reflect the greater warming east of the Date Line. Elements of this pattern (Fig. 2*c*) have also been noted in other studies of tropical Pacific SST trends over this period[3,19,20]. Thus in spite of the some differences in the patterns, both the model and observed trends indicate an overall tropical Pacific warming, with somewhat greater warming east of the Date Line, and a corresponding reduction of zonal SST gradient across the central tropical Pacific.

Associated with this reduction of meridional SST gradient, precipitation increased in the central equatorial Pacific and decreased in the warm-water regime regions of the Intertropical Convergence Zone (ITCZ), South Pacific Convergence Zone (SPCZ), Australasia, and the eastern Indian Ocean in the model (Fig. 3*a*). These mean climate-change patterns in the coupled model due to increased CO_2 resemble those associated with represent-day El Niño events in the tropical Pacific region[15,16], as well as similar changes observed during the 1980s[5,17]. Sea-level pressure (SLP) anomaly patterns from the coupled model, increased CO_2 minus control (Fig. 3*b*), also show the El Niño-like feature seen in the observations of an anomalously deepened Aleutian low-pressure centre in the north Pacific[21], as well as the similar decadal-timescale SLP anomalies in that region[2,4,22,23].

To examine in more detail the mechanisms producing these anomalies in the model, we compiled components of the surface energy balance and low-level moisture parameters for the tropical eastern and western Pacific Ocean areas for 20-year December–January–February averages (Table 1). The changes in SST near the time of CO_2 doubling in the model for these areas correspond to similar changes noted earlier (Fig. 1), with the eastern tropical Pacific area warming more (3.49 °C) than the western Pacific (2.21 °C).

Absorbed solar radiation at the surface decreases in the western Pacific area ($-3.92\,W\,m^{-2}$) and increases in the eastern Pacific area ($+2.23\,W\,m^{-2}$). This is due to cloud albedo feedback effects and changes in cloud amount (see Table 1). Warmer water increases albedo by 1% in the western Pacific area mainly due to cloud albedo feedback, even though total cloud amounts have decreased by 5% in association with the eastward shift of precipitation (Fig. 3). Decreased low clouds and corresponding increases in convective clouds with smaller cloud fraction in the eastern Pacific area contribute a decrease of total albedo by 4% (total cloud amount decreases by 13%, due to a decrease of low-level, predominantly stratus, clouds of 27%; middle- and upper-level, predominantly cumulus, clouds increase by 123%).

There are small changes in net infrared radiation and sensible (due to the temperature difference between the surface and overlying air) heat flux, but there is a large increase of latent heat flux (positive sign denotes heat removed from the ocean surface) in the eastern Pacific area compared to the western Pacific area ($+8.67\,W\,m^{-2}$ versus $+0.81\,W\,m^{-2}$). This is due to

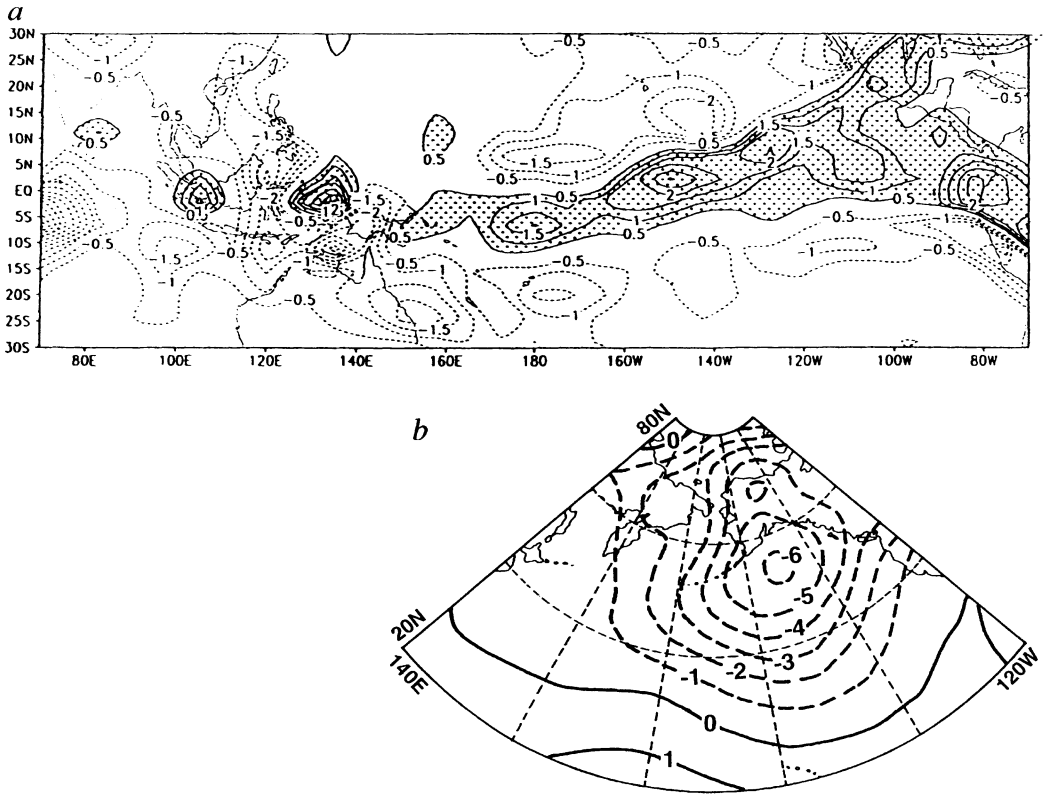

FIG. 3 *a*, Precipitation differences (mm d^{-1}), transient CO_2 increase experiment minus control, for December–January–February, the last 20 years of 75-year transient and control integrations with the coupled model (CO_2 has doubled in the atmosphere at about year 70 of the transient experiment), areas of precipitation increase are grey-shaded, and this pattern is similar to the precipitation anomalies during typical El Niño events[32]; note other coupled-model study of anomalously dry areas in the tropics during El Niño events becoming drier with increased CO_2 (ref. 34). *b*, Sea level pressure differences (m bar) for the north Pacific region, transient CO_2 increase experiment minus control, for December–January–February, the last 20 years of 75-year transient and control integrations with the coupled model (CO_2 has doubled in the atmosphere at about year 70 of the transient experiment).

greater evaporation in the eastern Pacific associated with larger SST increases, as well as relatively large increases of surface moisture (+16%) in the western Pacific that contribute to inhibiting larger evaporation increases there. There is also a large increase in low-level moisture convergence in the eastern Pacific area (+62%) compared to the western area (+3%). But, in absolute terms, there is still somewhat greater latent heat flux and low-level moisture amounts in the western Pacific area compared to the eastern area as observed[24,25], due to the higher base-state SSTs in the west[7]. Thus the changes in latent heat flux are the result of factors that produce an effect opposite to what would contribute to a reduction of zonal SST gradient.

Changes in ocean advection (mostly due to changes in upwelling; weak horizontal SST gradients in these particular regions do not contribute significantly to horizontal heat advection[7]) are larger for the eastern compared to the western Pacific area, indicating that the weakened easterlies and associated decreased upwelling (not shown) result in greater heating in the eastern Pacific (+7.56 W m^{-2} compared to +5.28 W m^{-2}) where upwelling is stronger in the present-day climate case.

Thus radiative changes (partly due to cloud albedo feedback, and partly due to changes in cloud amount), plus the large-scale dynamical atmosphere–ocean feedbacks that reduce the surface easterly winds and weaken equatorial upwelling in the ocean, combine to contribute to the greater relative warming of tropical Pacific SSTs east of the Date Line, with attendant precipitation and circulation anomalies, due to increased CO_2 in the coupled model. Droughts that already occur in the Australasia/western Pacific region in association with El Niño events could thus intensify, disrupting water resources on small islands dependent on rainfall for fresh water, and contributing to long-term depletion of those resources[6]. We cannot definitively attribute the recent warming in the Pacific (and associated global warming of the 1980s and early 1990s) to increased levels of CO_2 in the atmosphere. Yet the model results presented here and elsewhere[26,27], as well as some observational results[28], point to the possibility that CO_2-induced climate change in the Pacific region could have this signature. However, there may also be decadal-timescale variability in the tropical Pacific region that could complicate the interpretation of this signal (M. Latif, personal communication). Further clarification of these effects awaits more definitive observational and modelling studies, improved cloud formulations, and a better understanding of observed decadal-timescale climate fluctuations in the Pacific region. □

Received 12 June 1995; accepted 21 May 1996.

1. Nitta, T. & Yamada, S. *J. met. Soc. Japan* **67,** 375–383 (1989).
2. Trenberth, K. E. & Hurrell, J. W. *Clim. Dyn.* **9,** 303–319 (1994).
3. Graham, N. E. *Clim. Dyn.* **10,** 135–162 (1994).
4. Nitta, T. & Kachi, M. *J. met. Soc. Japan* **72,** 823–831 (1994).
5. Kumar, A., Leetma, A. & Ji, M. *Science* **266,** 632–634 (1994).
6. Meehl, G. A. *J. Wat. Air Soil Pollut.* (in the press).
7. Meehl, G. A. & Washington, W. M. *Clim. Dyn.* **11,** 399–411 (1995).
8. Ramanathan, V. & Collins, W. *Nature* **351,** 27–32 (1991).
9. Washington, W. M. & Meehl, G. A. *Clim. Dyn.* **8,** 211–223 (1993).
10. Boer, G. J. *Clim. Dyn.* **8,** 225–239 (1993).
11. Senior, C. A. & Mitchell, J. F. B. *J. Clim.* **6,** 393–418 (1993).
12. Houghton, J. T., Callander, B. A. & Varney, S. K. (eds) *Climate Change 1992: The IPCC Scientific Assembly Supplementary Report* (Cambridge Univ. Press, 1992).
13. Wallace, J. M. *Nature* **357,** 230–231 (1992).
14. Rasmusson, E. M. & Carpenter, T. H. *Mon. Weath. Rev.* **110,** 354–384 (1982).
15. Kiladis, G. N. & van Loon, H. *Mon. Weath. Rev.* **116,** 120–136 (1988).
16. Meehl, G. A. *Mon. Weath. Rev.* **115,** 27–50 (1987).
17. Salinger, J. M. *et al. Int. J. Climatology* **15,** 285–302 (1995).
18. Bottomly, M., Folland, C. K., Hsiung, J., Newell, R. E. & Parker, D. E. *Global Ocean Surface Temperature Atlas* (UK Met. Office, Bracknell, 1990).
19. Kitoh, A. *J. met. Soc. Japan* **73,** 247–253 (1995).
20. Gutzler, D. S. *J. atmos. Sci.* (in the press).
21. van Loon, H. & Madden, R. A. *Mon. Weath. Rev.* **109,** 1150–1162 (1981).
22. Trenberth, K. E. *Bull. Am. met. Soc.* **71,** 988–993 (1990).
23. Chen, T.-C., van Loon, H., Wu, D.-D. & Yen, M.-C. *J. met. Soc. Japan* **70,** 1137–1146 (1992).
24. Oberhuber, J. M. *An atlas Based on the COADS Data Set: The Budgets of Heat, Buoyancy and Turbulent Kinetic Energy at the Surface of the Global Ocean* (Max Planck Institute for Meteorology, Hamburg, 1988).
25. Zhang, G. J. & McPhaden, M. J. *J. Clim.* **8,** 589–605 (1995).
26. Knutson, T. R. & Manabe, S. *J. Clim.* **8,** 2181–2199 (1995).
27. Tett, S. *J. Clim.* **8,** 1473–1502 (1995).
28. Trenberth, K. E. & Hoar, T. J. *Geophys. Res. Lett.* **23,** 57–60 (1996).
29. Folland, C. K., Parker, D. E. & Kates, F. E. *Nature* **310,** 670–673 (1984).
30. Folland, C. K. & Parker, D. E. *Climate–Ocean Interaction* 21–52 (Kluwer, Dordrecht, 1990).
31. Meehl, G. A., Branstator, G. W. & Washington, W. M. *J. Clim.* **6,** 42–63 (1993).
32. Ropelewski, C. F. & Halpert, M. S. *Mon. Weath. Rev.* **115,** 1606–1626 (1987).
33. Alexander, R. C. & Mobley, R. L. *Mon. Weath. Rev.* **104,** 143–148 (1976).
34. Meehl, G. A. & Washington, W. M. *Mon. Weath. Rev.* **114,** 667–674 (1986).
35. Graham, N. *Science* **267,** 666–671 (1995).

ACKNOWLEDGEMENTS. We thank M. Latif for comments and for providing the observed SST trend map, and J. Hurrell for his comments. Some of the computations were performed under the auspices of the Model Evaluation Consortium for Climate Assessment (MECCA) and CRAY Research, Inc. The National Center for Atmospheric Research is sponsored by the National Science Foundation. This work was supported in part by the US Department of Energy, Office of Health and Environmental Research as part of its Carbon Dioxide Research Program.

CORRESPONDENCE should be addressed to G.A.M. (e-mail meehl@ncar.ucar.edu).

Life and times of the Bering land bridge

Scott A. Elias*, Susan K. Short*, C. Hans Nelson† & Hilary H. Birks‡

* Institute of Arctic and Alpine Research, Campus Box 450, University of Colorado, Boulder, Colorado 80309-0450, USA
† US Geological Survey, Mail Stop 999, Menlo Park, California 94025, USA
‡ Botanical Institute, University of Bergen, Allegaten 41, N-5007 Bergen, Norway

UNDERSTANDING the environment of the Bering land bridge and determining the timing of late Wisconsin inundation are important for several areas of study. These include: (1) the timing of the re-establishment of circulation between Pacific and Atlantic Oceans; (2) the timing of development of a northern biotic refugium and the closing of the bridge to species immigration; (3) Palaeoindian migration routes; and (4) palaeotopographic data for atmospheric general circulation models[1]. Late Wisconsin palaeobotanical and fossil insect data from the central and northern sectors of the Bering land bridge indicate widespread mesic shrub tundra environments even during the last glacial maximum. Contrary to previous hypotheses, we found no evidence of steppe tundra on the land bridge. New accelerator mass spectrometer ^{14}C dates show much of the land bridge was above sea level and thus available for human and animal migration until 11,000 yr BP. Insect evidence suggests that summer temperatures at that time were substantially warmer than now.

The reconstruction of full-glacial vegetation of Beringia has been controversial[2–5]. The hypothesis of a productive grassland was based on fossils of large grazers in full-glacial sediments. High percentages of *Artemisia* in Beringian pollen spectra were interpreted as being attributable to a steppe tundra or mammoth steppe, dominated by plants found in Asian steppes today[4]. The steppe-tundra hypothesis has been questioned on the basis of palynology[2,3,5]. Prior reconstructions of lowland environments on the land bridge have been based on extrapolation from adjoining upland regions, so no definitive evidence for the full-glacial vegetation of the land bridge has been available.

We analysed 20 cores collected by the US Geological Survey from the Bering and Chukchi Seas for beetles, pollen, and plant macrofossils to reconstruct environments during the last glaciation (Fig. 1). The organic strata, ranging in thickness from <5 to 300 cm, were *in situ* terrestrial peats and organic detrital silts formed on the emergent land bridge, subsequently overlain by Holocene marine sediments from marine transgression.

Radiocarbon dates from these cores range in age from 3,455 to >49,200 yr BP (Table 1). New accelerator mass spectrometer (AMS) ages from peat near the top of non-marine sediment on the Chukchi shelf suggest that the previous conventional radiocarbon ages on bulk sediments were as much as 4.25 kyr too old[6].

McManus and Creager[7] estimated that the land bridge was inundated by 14,400 ^{14}C yr BP. However, their sea-level chronology is suspect because it was based on radiocarbon ages of bulk